Sub Topic: Laminar Flames

12<sup>th</sup> U.S. National Combustion Meeting Organized by the Central States Section of the Combustion Institute May 24–26, 2021 (Virtual) College Station, Texas

# Schlieren-based measurements of propane flame speeds at extreme temperatures

Adam J. Susa<sup>1,\*</sup>, Lingzhi Zheng<sup>1</sup>, and Ronald K. Hanson<sup>1</sup>

<sup>1</sup>Mechanical Engineering, Stanford University, Stanford, CA, United States

\*Corresponding author: asusa@stanford.edu

**Abstract:** Flame speed measurements of stoichiometric ( $\phi$ =1) propane in an oxygen-argon oxidizer (21% O<sub>2</sub>, 79% Ar) were conducted behind reflected shock waves at unburned-gas temperatures from 800 K to nearly 1,200 K. As in previous shock-tube flame speed experiments, non-intrusive laser-induced breakdown is used to ignite an expanding flame in the nominally quiescent gas following the reflected-shock passage. In addition to the end-wall emission imaging employed in previous works, a schlieren imaging diagnostic is employed utilizing side-wall optical ports. The high temporal and spatial resolutions of the schlieren diagnostic allow for measurements to be made of small, curvature-stabilized flames (r < 7 mm) with short measurement times (t < 600  $\mu$ s). Direct comparison of simultaneous emission- and schlieren-based measurements illustrates that measurements performed with the two techniques agree at comparable flame radii. The comparison further shows the schlieren-based measurements do not show evidence of flame acceleration as is seen in the emission-based measurements at larger flame radii and longer measurement times. Extrapolated, zero-stretch flame speeds are compared with those calculated using detailed and reduced reaction mechanisms, accounting for auto-ignition chemistry effects in accordance with the recent literature.

Keywords: Flame speed, Shock tube, Propane, Schlieren

### 1. Introduction

At the extreme conditions reached within modern combustion engines, flame propagation and spontaneous ignition chemistry can occur simultaneously, coupling with one another to jointly govern engine operability and performance [I]. Zeldovich was the first to explicitly consider the effect of reactions in a preheated substance on the flame propagation speed, determining that a continuum of solutions to the chemistry-affected deflagration speeds are possible, bounded from below by the unaffected flame speed [2]. Nevertheless, such chemistry-affected deflagrations are governed by heat conduction and diffusion, making them distinct from the spontaneous propagation regime governed by nonuniform initial conditions [3].

Recently, a growing number of efforts to predict the behavior of laminar flames at autoigniting unburned-gas conditions have been reported, employing simulation-based methods of varying complexity [e.g.  $\boxed{1}$ ,  $\boxed{4}$ - $\boxed{9}$ ]. However, while significant advancements have been made in extending the range of pressures accessible to flame speed measurement [e.g.  $\boxed{10}$ ,  $\boxed{11}$ ], practical limitations have made progress in extending the experimentally accessible temperature range more protracted. To the authors' knowledge, the 873-K measurements reported by Kurata et al.  $\boxed{12}$ ] represent the highest unburned-gas temperature ( $T_u$ ) reported in the literature, measurements made using a

Bunsen-flame configuration that has since fallen out of favor due to high experimental uncertainties [13]. The confined spherically expanding flame (CSEF) method has been demonstrated up to 720 K [14]. While the CSEF method conveniently provides simultaneously elevated pressure and temperature, the unburned-gas compression can also lead to end-gas autoignition [15], capping the range of conditions accessible to flame speed measurement. The heated, diverging channel method has been employed in flame speed measurements up to about 650 K [e.g. [16]], conditions above which turbulence and uncontrolled gas reactivity are encountered. Reactor assisted turbulent slot (RATS) burners have been used in the measurement of turbulent flame speeds at  $T_{\rm u}$  up to about 700 K, but remain dependent on simulated laminar flame speeds to interpret the results [e.g. [17]].

The shock-tube flame speed method, first reported by Ferris et al. [18], brought promise for unlocking experimental study at never-before-accessible, high-temperature conditions. Following the initial demonstration of propane flame speeds up to 832 K, the method was applied to by Susa et al. in studies reporting the first experimental evidence of negative temperature dependence in *iso*-octane flame speeds [19] and the behavior of *n*-heptane flames at controlled extents of unburned-gas reaction [20]. In the various prior works, the observation of instabilities has limited the highest-temperature conditions at which flame speed could be measured. This work reports significant progress in overcoming this limitation, wherein the implementation of a new schlieren-imaging diagnostic and experimental refinements, informed by recent efforts to characterize the post-shock flow field [21], allow for extrapolated stretch-free flame speeds to be reported at extreme unburned-gas temperatures up to 1,190 K for the first time.

# 2. Experimental Methodology

# 2.1 Experimental Setup

Flames are generated in a shock tube following the general methodology introduced by Ferris et al. [18]. The shock tube, described by Campbell et al. [22], features a 11.53-cm inner diameter, 9.76-m driven section, and variable length driver to accommodate long test times. Stoichiometric ( $\phi$ = 1) mixtures of propane ( $C_3H_8$ ) in an oxidizer comprised of 21% oxygen ( $O_2$ ) and 79% argon (Ar) are prepared manometrically in a stainless-steel mixing tank before being introduced into the evacuated shock-tube driven section. The mixtures are subsequently heated and pressurized by reflected shock waves to post-reflected-shock (region-5), unburned-gas conditions of  $P_u \approx 1$  atm and temperatures in the range 800 K <  $T_u$  < 1,200 K.

Eight ports provide optical access to the 2-cm measurement plane in which flames are generated in this work. This change from prior works, in which flames were studied at 10 cm from the end wall, is intended to reduce the magnitude of any post-reflected-shock gas motion. A quartz end wall provides axial optical access for emission imaging [23]. A Kistler pressure transducer provides high-speed pressure measurements, while a 3.41-µm laser absorption diagnostic [24] enables in-situ verification of the manometric fuel-loading. Figure [1] displays schematics of the instrumentation configuration used in this work from the top-down and end-on perspectives.

A schlieren imaging diagnostic is implemented utilizing the optical access provided by 18-mm-diameter side-wall-port windows. A high-power light-emitting diode (LED) provides the illumination source. One-inch-diameter, 250-mm-focal-length mirrors (f/10) arranged in a z-fold optical arrangement collimate and refocus the light; an extra, flat mirror is included to fold the optical system for compactness. A vertically oriented slit positioned at the catch-side focal point serves

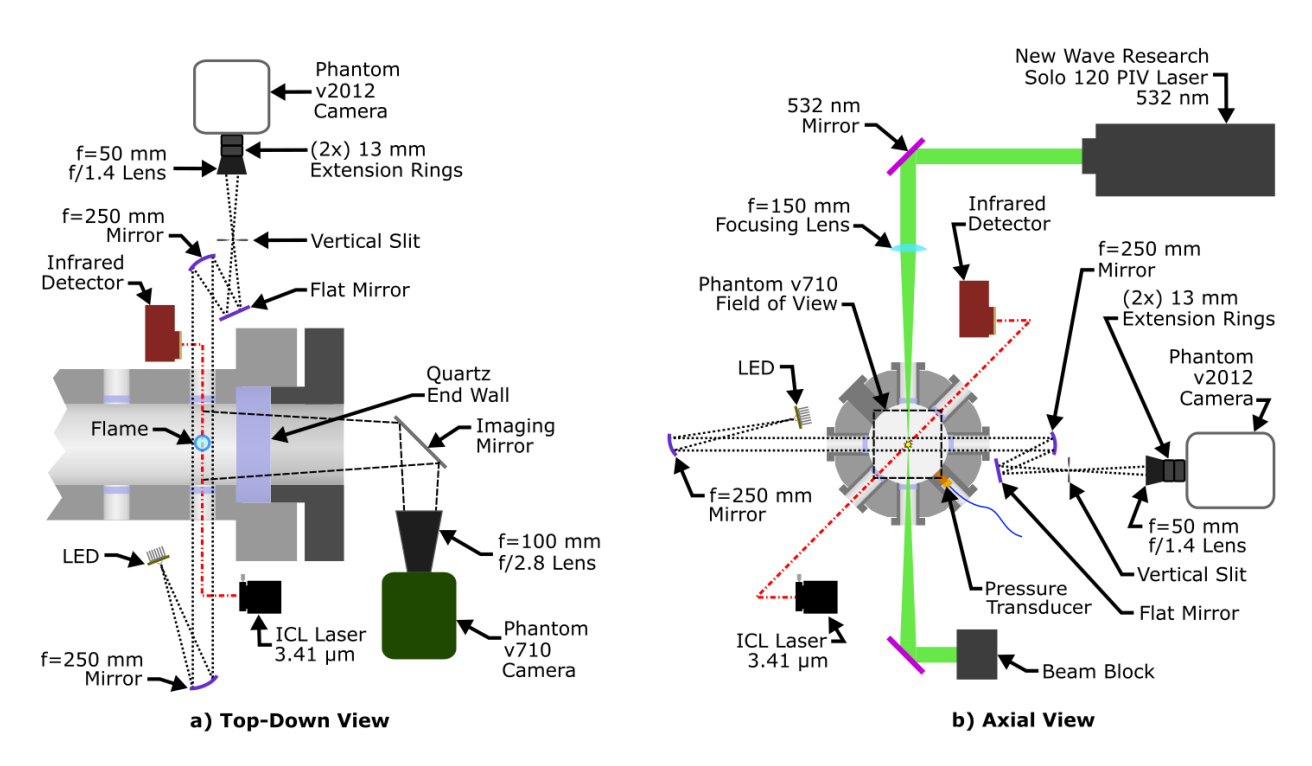


Figure 1: Schematic of the instrumentation used in this work, as viewed from a) the top and b) the end of the tube, with the shock tube shown in cross section. Schlieren optical path shown out of plane in axial view for clarity. Schematic not to scale.

as the schlieren stop. The use of a slit, as opposed to the more conventional knife edge, results in relatively low contrast, but symmetry between positive and negative density gradients.

A high-speed, Phantom v2012 camera (Vision Research) records the schlieren images through a 50-mm-focal-length, f/1.4 Nikon lens offset by a pair of 13-mm extension rings. Schlieren images are recorded by a reduced 128x96-pixel region of the sensor at 500,000 frames per second (fps) and a spatial resolution of 153 µm per pixel; The high-intensity LED source enables use of a short, 300-ns exposure time, effectively eliminating any motion blur.

End-wall emission imaging is performed simultaneously using a Phantom v710 camera (Vision Research). The unfiltered, unintensified camera records broadband, visible emission from electronically excited species (e.g. CH\*,  $C_2$ \*) produced by the flame. The v710 camera is aligned to image nearly the entire shock-tube onto a reduced, 544x536-pixel sensor region at 20,000 frames per second and 165  $\mu$ m per pixel resolution. Primary exposure times of 5 to 10  $\mu$ s were found to provide adequate signal for flame images; the extreme-dynamic range (EDR) exposure is set to 1  $\mu$ s to avoid overexposure during autoignition events.

Flames are ignited non-intrusively by a laser-induced plasma spark. A q-switched, frequency-doubled (532-nm), neodymium-doped yttrium aluminum garnet (Nd:YAG) laser (Solo PIV 120, New Wave Research) serves as the laser source. A 150-mm-focal-length, best-form spherical lens focuses the beam to a waist at the center of the tube, defining the location at which laser-induced breakdown occurs. Pulse-energy control is achieved by externally triggering the q-switch at a controlled time after the flash lamp. In the present work, a delay of 114 µs produces 14-18 mJ per pulse, of which an estimated 8-12 mJ was deposited in the plasma spark.

#### 2.2 Image Processing

The first step employed in processing the schlieren images is to apply noise-rejecting filters. Image sequences are sequentially filtered with temporal median and mean filters with spans of five frames to reject noise without spatially blurring the images (Fig. 2a). To extract the weak schlieren signal from the background, the optical density, OD, of the schlieren images is calculated pixel-wise following Eqn. 1.

 $OD = -\ln\left(\frac{I_{\text{img}}}{I_{\text{bkgd}}}\right) \tag{1}$ 

In Eqn.  $\boxed{1}$ ,  $I_{\rm img}$  is the intensity of the filtered schlieren images and  $I_{\rm bkgd}$  is that of the background image. When a single, pre-flame background image is used, background intensity fluctuations throughout an experiment are found to introduce objectionable noise and artifacts into the OD images (Fig.  $\boxed{2}$ b). To overcome this challenge, a rolling-average, skip-gap background image is instead used, wherein the background is taken as the average over a number of frames prior to and following the image of interest, offset by a number of buffer frames. This scheme effectively rejects relatively slow variations in the background while enhancing relatively fast moving features, most notably the flame front (Fig.  $\boxed{2}$ c).

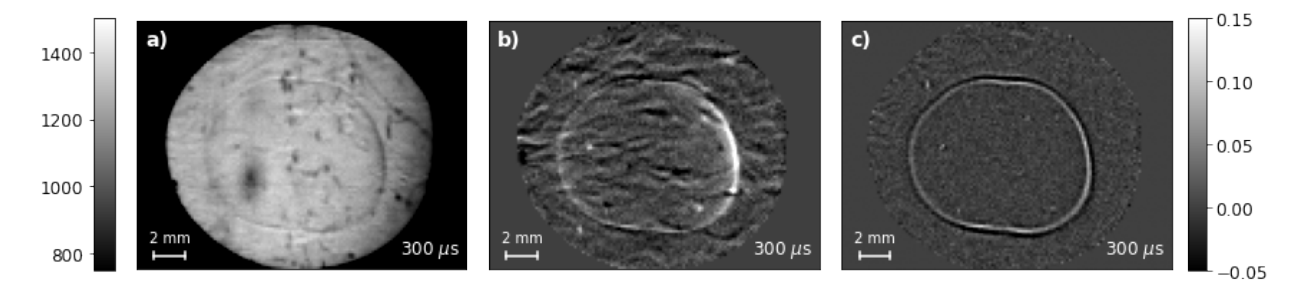


Figure 2: a) Temporally filtered image from a  $T_u = 988$  K flame experiment. Corresponding OD images calculated against a b) pre-flame and c) skip-gap, rolling-average background image. Right intensity scale applies to both OD images (b) and (c). Timestamps shown relative to spark.

Flame fronts are extracted directly from OD images using an active contour model in which a closed contour is optimized to follow the maximum image intensity [25]. Figure [3a,b] shows the resulting flame contours of the first and last schlieren images from which flame fronts are extracted. A 100-point contour is first initialized using a OD image binarized with hysteresis thresholding [26] and smoothed with a Gaussian filter. The last frame with the flame fully in the field of view is used for the initialization, as binarization is found to be more robust for later frames than early frames. After initializing to the binary image, the contour is re-optimized to the original OD image (Fig. [3b). Each subsequent OD image, working backwards from the last frame, is then sequentially contoured, with the previous optimal contour serving as the starting point for the following frame. The points describing each contour are mapped to radial coordinates relative to their centroid, providing measures of the flame radius at various angular locations,  $r_{\rm f,\theta}$ , for each frame.

Emission images are treated similarly to schlieren images, with minor adjustments. A temporal median filter is applied to the image sequences; mean filtering is not used to avoid introducing

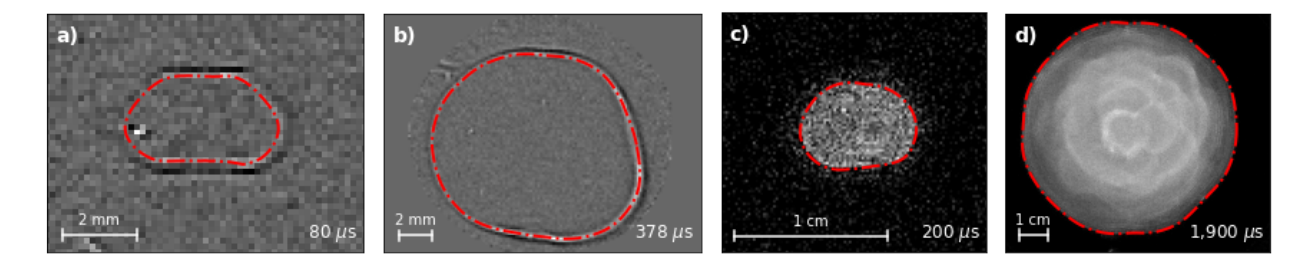


Figure 3: First and last flame contours (red dashed lines) overlaid on the corresponding (a, b) schlieren OD images (c, d) and emission images. The first frame of each image type (a, c) is shown zoomed for clarity, whereas (b, d) display the full recorded image region. All images taken from the same  $T_u = 988$  K experiment. Timestamps shown relative to spark.

motion blur to the images. Background subtraction is next employed using the average of the preflame images as the background. A binarized edge of the final frame is used to initialize a contour, which then optimized directly to the emission images with the optimization parameter of the active contour model set to follow the maximum intensity gradients (Fig. 3c-d). As is apparent in Fig. 3d, flames exhibit significant cellularity at large radii not seen in the schlieren images obtained at much smaller radii. For this reason, emission-based measurement are included in Sec. 3 only for qualitative comparison to the schlieren results and are not included in the data extrapolations.

# 2.3 Data Interpretation

In a simple interpretation, the flame radius,  $r_{\rm f}$ , for each image can be estimated as an average over the  $r_{\rm f,\theta}$  defining the optimal contour. This definition does not account for aspherical geometry, but is considered to be a reasonable first-order approximation for the flames observed in the schlieren images for which measurements are reported. In the limit of a spherical, expanding flame, the burned flame speed,  $S_{\rm b}$ , can be taken as the time derivative of  $r_{\rm f}$ ,

$$S_{b} = \frac{\mathrm{d}r_{\mathrm{f}}}{\mathrm{d}t}.\tag{2}$$

A Savitzky-Golay filter [27] is used to calculate the derivative of the radius—time data with window sizes of 11 and 3 for the schlieren and emission data, respectively.

Extrapolation of the measured flames speeds to zero stretch is performed using the linear-curvature (LC) model first proposed by Markstein [28],

$$S_{b} = S_{b}^{0} - S_{b}^{0} L_{b} \left(\frac{2}{r_{f}}\right). \tag{3}$$

In Eqn.  $\boxed{3}$ ,  $S_b^0$  is the burned, stretched flame speed,  $L_b$  is the Markstein length, and  $(2/r_f)$  is the flame curvature in the limit of a spherical flame. The selection of the LC model is motivated by the works of Chen  $\boxed{29}$  and Cai et al.  $\boxed{30}$ , who have shown the LC model more closely captures both the theoretical and numerically simulated burning behavior of flames with Le > 1 than alternative models and allows for the extraction of flame speeds from highly stretched flame kernels.

Extrapolated, zero-curvature (i.e. zero-stretch) flame speeds are converted from the burned reference frame to that of the unburned gas using the density ratio,

$$S_{\rm u}^0 = \left(\frac{\rho_{\rm b}}{\rho_{\rm u}}\right) S_{\rm b}^0,\tag{4}$$

an oft-employed relation based upon continuity of the mass burning flux. The unburned-gas density,  $\rho_u$ , is calculated at the known post-reflected-shock conditions; the burned-gas density,  $\rho_b$ , is estimated as the density at thermo-chemical equilibrium.

#### 3. Results and Discussion

The results of stoichiometric propane/ $O_2$ /Ar flame speed measurements for unburned-gas temperatures in the range of 806 K to 1,190 K are presented in Fig. 4 Linear extrapolations of the  $S_b$  vs. curvature schlieren data to zero curvature are additionally presented. Pairs of experiments performed at nearly matched conditions near 990 K and 1,090 K show close agreement. Emission-based measurements show notable flame acceleration at larger flame radii, consistent with the qualitative observation of flame-front instability observed in the emission images.

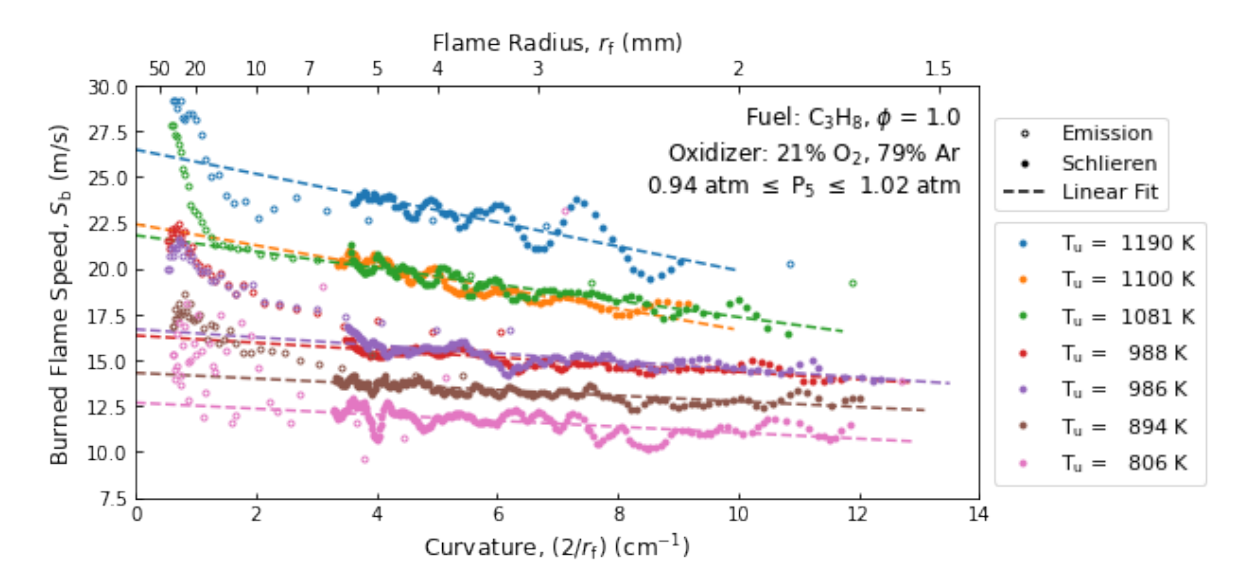


Figure 4:  $S_b$  vs. curvature measurements obtained from shock tube flame speed experiments. Measurements are shown as obtained from emission (open circle) and schlieren (closed circle) images, which show satisfactory agreement at overlapping curvatures. Linear fits (dashed lines) are based only upon the schlieren results and shown extrapolated to zero curvature.

Extrapolated values of  $S_u^0$  and  $L_b$  are shown in Fig. 5, alongside laminar flame speeds  $S_L$  calculated using Chemkin-Pro with several kinetic mechanisms and various domain lengths for comparison. Recent works have shown that steady-state flame solutions can provide both domain-length insensitive  $S_L$  values when the domain length is kept sufficiently small; increasing the domain length, and with it the pre-flame residence time, provides a simple manner of accounting for autoignition chemistry [e.g. 4-6]. Simulated flame speeds with 1-cm domains fall in the

domain-length insensitive regime for all mechanisms shown, whereas the 5-cm and 7.5-cm domains provide sufficient residence time to allow non-negligible pre-flame autoignition chemistry at the highest temperatures, evidenced by the increases in  $S_L$ . The maximum uncertainties of  $S_b^0$  and  $L_b$  based on linear fits of the schlieren data are 2.3% and 18.4%, respectively, calculated at the 95% confidence level; corresponding error bars are included for all data point in Fig. 5 but are too small to be seen for all but the highest-temperature value of  $S_u^0$ .

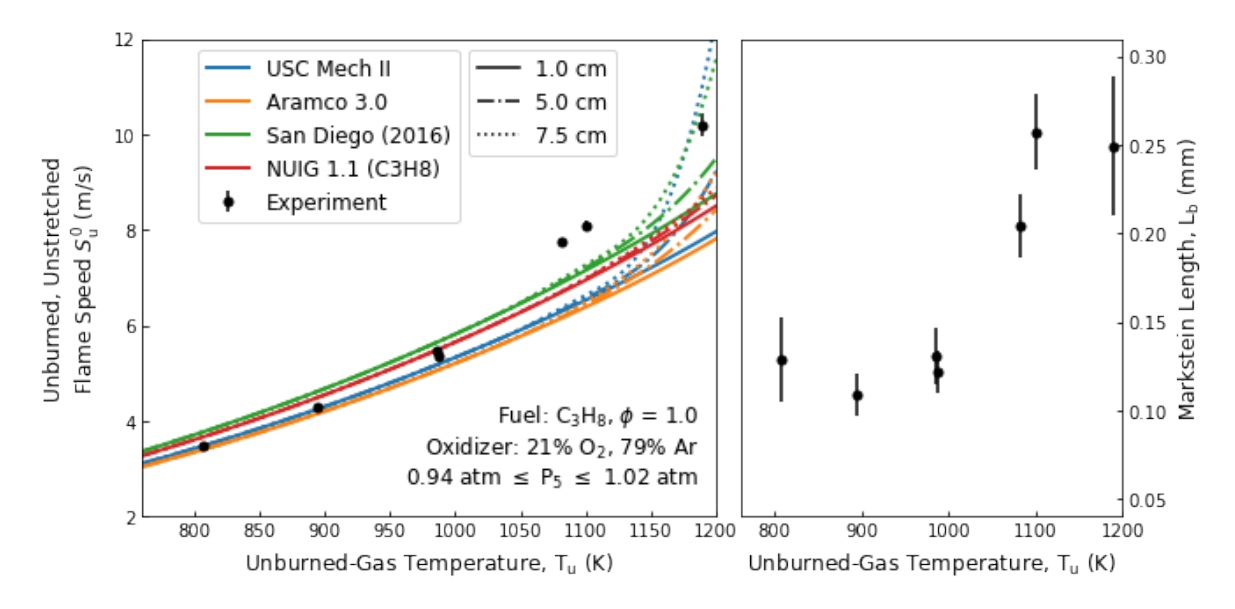


Figure 5: Extrapolated unburned, zero-curvature flame speeds (left) and Markstein lengths (right) for extreme-temperature flames measured in this work. Modeled laminar flame speeds with varying domain lengths are shown for comparison.

For  $T_{\rm u} \lesssim 900$  K, experimentally derived  $S_{\rm u}^0$  values agree well with  $S_{\rm L}$  values calculated using the USC Mech. II [31] and Aramco 3.0 [32] mechanisms, while the 2016 San Diego mechanism [33] and a single-fuel, skeletal propane mechanism derived from NUIGMech 1.1 [34] both overpredict  $S_{\rm u}^0$ . Experimental results fall between values simulated with the various mechanisms for measurement with  $T_{\rm u}$  near 1,000 K. Above 1,000 K, experimental  $S_{\rm u}^0$  results exceed the domain-length-insensitive (1-cm)  $S_{\rm L}$  values of all mechanisms; this deviation comes in conjunction with an increase in  $L_{\rm b}$  values, from between 0.1-0.15 mm for  $T_{\rm u} \lesssim 1,000$  K to 0.2-0.26 mm for higher  $T_{\rm u}$ . Increasing the domain length to 7.5 cm is insufficient to replicate this discrepancy for results near 1,100 K. Flame speeds calculated with the USC Mech II and San Diego mechanisms are sufficiently accelerated by pre-flame chemistry in a 7.5-cm domain to exceed the 1,190 K measurement. However, the corresponding residence time in the simulation ( $\approx 3$  ms) is significantly longer than the time required to complete the highest-temperature measurement in the shock tube ( $\approx 600$  µs). As such, the discrepancies between the highest-temperature experiments and simulations cannot be explained by the residence-time effect alone, warranting further investigation.

#### 4. Conclusions

Flame speed measurements at extreme temperatures in excess of 1,000 K are reported for the first time. The measurements are performed using a high-speed schlieren imaging diagnostic optimized

record small, curvature-stabilized flames. Experimental refinements are additionally employed, including the use of the 2-cm measurement plane and using Ar as the sole diluent. Extrapolated  $S_{\rm u}^0$  values are compared to  $S_{\rm L}$  computed with several combustion mechanisms, allowing for the effects of autoignition chemistry. Measured  $S_{\rm u}^0$  values agree well with USC Mech. II and Aramco Mech. 3.0 up to 1,000 K. Above 1,000 K, an increase in the observed  $L_{\rm b}$  is observed, and experimental  $S_{\rm u}^0$  results are found to exceed simulated  $S_{\rm L}$  values, except for when unrealistically long pre-flame residence times are considered. As such, the effect of autoignition chemistry, as provided for with the simulation method and mechanisms considered in this work, is found to be insufficient to account for experimentally measured results, motivating future work to elucidate the causes of the discrepancy at these previously inaccessible, extreme-temperature conditions.

## 5. Acknowledgments

This work was supported by the U.S. National Science Foundation under award number 1940865, contract monitors Dr. Harsha Chelliah (former) and Dr. John Daily (current). A. J. Susa recognizes the U.S. Department of Defense for financial support through a NDSEG Fellowship.

### References

- [1] K. V. Puduppakkam, A. U. Modak, C. Wang, D. Hodgson, C. V. Naik, and E. Meeks, Generating Laminar Flame Speed Libraries for Autoignition Conditions, Turbo Expo: Power for Land, Sea, and Air (2020), V04BT04A004, DOI: 10.1115/GT2020-15274.
- Y. Zeldovich, Flame propagation in a substance reacting at initial temperature, Combustion and Flame 39 (1980) 219–224. DOI: 10.1016/0010-2180(80)90019-X.
- [3] Y. B. Zeldovich, Regime classification of an exothermic reaction with nonuniform initial conditions, Combustion and Flame 39 (1980) 211–214. DOI: 10.1016/0010-2180(80) 90017-6.
- [4] R. Sankaran, Propagation velocity of a deflagration front in a preheated autoigniting mixture, In 9th US National Combustion Meeting (2015).
- [5] J. Pan, H. Wei, G. Shu, Z. Chen, and P. Zhao, The role of low temperature chemistry in combustion mode development under elevated pressures, Combustion and Flame 174 (2016) 179–193. DOI: 10.1016/j.combustflame.2016.09.012.
- [6] A. Krisman, E. R. Hawkes, and J. H. Chen, The structure and propagation of laminar flames under autoignitive conditions, Combustion and Flame 188 (2018) 399–411. DOI: 10.1016/j.combustflame.2017.09.012.
- [7] A. Ansari, J. Jayachandran, and F. N. Egolfopoulos, Parameters influencing the burning rate of laminar flames propagating into a reacting mixture, Proceedings of the Combustion Institute 37 (2019) 1513–1520. DOI: 10.1016/j.proci.2018.05.163.
- [8] M. Faghih, H. Li, X. Gou, and Z. Chen, On laminar premixed flame propagating into autoigniting mixtures under engine-relevant conditions, Proceedings of the Combustion Institute 37 (2019) 4673–4680. DOI: 10.1016/j.proci.2018.06.058.

- [9] T. Zhang, A. J. Susa, R. K. Hanson, and Y. Ju, Studies of the dynamics of autoignition assisted outwardly propagating spherical cool and double flames under shock-tube conditions, Proceedings of the Combustion Institute (2020), DOI: 10.1016/j.proci.2020.06.089.
- [10] S. D. Tse, D. Zhu, and C. K. Law, Morphology and burning rates of expanding spherical flames in H2/O2/inert mixtures up to 60 atmospheres, Proceedings of the Combustion Institute 28 (2000) 1793–1800. DOI: 10.1016/S0082-0784(00)80581-0.
- [11] C. Xiouris, T. Ye, J. Jayachandran, and F. N. Egolfopoulos, Laminar flame speeds under engine-relevant conditions: uncertainty quantification and minimization in spherically expanding flame experiments, Combustion and Flame 163 (2016) 270–283. DOI: 10.1016/j.combustflame.2015.10.003.
- [12] O. Kurata, S. Takahashi, and Y. Uchiyama, Influence of preheat temperature on the laminar burning velocity of methane-air mixtures, SAE transactions (1994) 1766–1772. DOI: 10. 4271/942037.
- [13] F. N. Egolfopoulos, N. Hansen, Y. Ju, K. Kohse-Höinghaus, C. K. Law, and F. Qi, Advances and challenges in laminar flame experiments and implications for combustion chemistry, Progress in Energy and Combustion Science 43 (2014) 36–67. DOI: 10.1016/j.pecs. 2014.04.004.
- [14] Y. Wang, A. Movaghar, Z. Wang, Z. Liu, W. Sun, F. N. Egolfopoulos, and Z. Chen, Laminar flame speeds of methane/air mixtures at engine conditions: performance of different kinetic models and power-law correlations, Combustion and Flame 218 (2020) 101–108. DOI: 10. 1016/j.combustflame.2020.05.004.
- [15] R. Lawson, V. Gururajan, A. Movaghar, and F. N. Egolfopoulos, Autoignition of reacting mixtures at engine-relevant conditions using confined spherically expanding flames, Proceedings of the Combustion Institute (2020), DOI: 10.1016/j.proci.2020.06.224.
- [16] M. Akram and S. Kumar, Measurement of laminar burning velocity of liquified petrolium gas air mixtures at elevated temperatures, Energy & fuels 26 (2012) 3267–3274. DOI: 10.1021/ef300101n.
- [17] S. H. Won, B. Windom, B. Jiang, and Y. Ju, The role of low temperature fuel chemistry on turbulent flame propagation, Combustion and Flame 161 (2014) 475–483. DOI: 10.1016/j.combustflame.2013.08.027.
- [18] A. M. Ferris, A. J. Susa, D. F. Davidson, and R. K. Hanson, High-temperature laminar flame speed measurements in a shock tube, Combust. Flame 205 (2019) 241–252. DOI: 10.1016/j.combustflame.2019.04.007.
- [19] A. J. Susa, A. M. Ferris, D. F. Davidson, and R. K. Hanson, Experimental Observation of Negative Temperature Dependence in iso-Octane Burning Velocities, AIAA Journal 57 (2019) 4476–4481. DOI: 10.2514/1.J058530.
- [20] A. J. Susa, A. M. Ferris, D. F. Davidson, and R. K. Hanson, Experimental measurement of laminar burning velocity of n-heptane at variable extents of reactions in a shock tube, Int. Symp. on Shock Waves 32 (2019), DOI: 10.3850/978-981-11-2730-4\_0149-cd.

- [21] A. J. Susa and R. K. Hanson, Flame-drift velocimetry and flame morphology measurements with dual-perspective imaging in a shock tube, In 12th US National Combustion Meeting (2021).
- [22] M. Campbell, A. Tulgestke, D. Davidson, and R. Hanson, A second-generation constrained reaction volume shock tube, Review of Scientific Instruments 85 (2014) 055108. DOI: 10.1063/1.4875056.
- [23] V. Troutman, C. Strand, M. Campbell, A. Tulgestke, V. Miller, D. Davidson, and R. Hanson, High-speed OH\* chemiluminescence imaging of ignition through a shock tube end-wall, Applied Physics B 122 (2016) 56. DOI: 10.1007/s00340-016-6326-y.
- [24] S. Wang, T. Parise, S. E. Johnson, D. F. Davidson, and R. K. Hanson, A new diagnostic for hydrocarbon fuels using 3.41-um diode laser absorption, Combustion and Flame 186 (2017) 129–139. DOI: 10.1016/j.combustflame.2017.07.026.
- [25] M. Kass, A. Witkin, and D. Terzopoulos, Snakes: Active contour models, International journal of computer vision 1 (1988) 321–331. DOI: 10.1007/BF00133570.
- [26] J. Canny, A Computational Approach to Edge Detection, IEEE Transactions on Pattern Analysis and Machine Intelligence PAMI-8 (1986) 679–698. DOI: 10.1109/TPAMI.1986. 4767851.
- [27] A. Savitzky and M. J. Golay, Smoothing and differentiation of data by simplified least squares procedures. Analytical chemistry 36 (1964) 1627–1639. DOI: 10.1021/ac60214a047.
- [28] G. H. Markstein, Experimental and theoretical studies of flame-front stability, Journal of the Aeronautical Sciences 18 (1951) 199–209. DOI: 10.2514/8.1900.
- [29] Z. Chen, On the extraction of laminar flame speed and Markstein length from outwardly propagating spherical flames, Combustion and Flame 158 (2011) 291–300. DOI: 10.1016/j.combustflame.2010.09.001.
- [30] X. Cai, J. Wang, H. Zhao, Y. Xie, and Z. Huang, Effects of initiation radius selection and lewis number on extraction of laminar burning velocities from spherically expanding flames, Combustion Science and Technology 190 (2018) 286–311. DOI: 10.1080/00102202. 2017.1389912.
- [31] H. Wang, X. You, A. V. Joshi, S. G. Davis, A. Laskin, F. Egolfopoulos, and C. K. Law, USC Mech Version II. High-temperature combustion reaction model of H2/CO/C1-C4 compounds, (2007), URL: http://ignis.usc.edu/USC\_Mech\_II.htm.
- [32] C. W. Zhou and et al., An experimental and chemical kinetic modeling study of 1, 3-butadiene combustion: Ignition delay time and laminar flame speed measurements, Combustion and Flame 197 (2018) 423–438. DOI: 10.1016/j.combustflame.2018.08.006.
- [33] U. of California at San Diego, *Chemical-Kinetic Mechanisms for Combustion Applications*, 2016, URL: http://web.eng.ucsd.edu/mae/groups/combustion/mechanism.html.
- [34] Q.-D. Wang, S. Panigrahy, S. Yang, S. Martinez, J. Liang, and H. J. Curran, Development of Multipurpose Skeletal Core Combustion Chemical Kinetic Mechanisms, Energy & Fuels (2021), DOI: 10.1021/acs.energyfuels.1c00158.